JOURNAL OF GEOPHYSICAL RESEARCH, VOL. 107, NO. D17, 4330, doi:10.1029/2001JD001156, 2002

A three-dimensional model of molecular hydrogen in the troposphere

D. A. Hauglustaine
Service d'Aéronomie du CNRS, Université de Paris 6, Paris, France
Laboratoire des Sciences du Climat et de l'Environnement, Gif-sur-Yvette, France

D. H. Ehhalt
Institut für Atmosphärische Chemie, Forschungszentrum Jülich, Jülich, Germany

Received 31 July 2001; revised 14 December 2001; accepted 2 January 2002; published 11 September 2002.

[1] The global distribution and budget of atmospheric molecular hydrogen (H_2) is simulated with a global Chemistry-Transport Model (CTM). Surface emissions include technological sources (industry, transportation and other fossil fuel combustion processes), biomass burning, nitrogen fixation in soils, and oceanic activity and totals 39 Tg/yr. The photochemical production (31 Tg/yr) from formaldehyde photolysis accounts for about 45% of the total source of H_2. Soil uptake (55 Tg/yr) represents a major loss process for H_2 and contributes for 80% to the total destruction. H_2 oxidation by OH in the troposphere contributes the remainder. The global burden of H_2 in the atmosphere is 136 Tg. Its overall lifetime in the atmosphere is 1.9 years. H_2 is rather well-mixed in the free troposphere. However, its distribution shows a significant seasonal variation in the lower troposphere where soil uptake dominates. This loss process shows a strong temporal variability and is maximum over the northern hemisphere landmass during summer. Strong vertical gradients result from this surface uptake. In these regions, H_2 varies by more than 30% between the maximum mixing ratio in winter and the summer minimum. Our results stress the important role played by the tropics in the budget of H_2. In these regions a strong seasonal cycle is also predicted due to the annual variation in biomass burning emissions, soil uptake, and rapid transport by convection of H_2 depleted air masses from the boundary layer to the upper troposphere. A comparison with the observed H_2 distribution allows to test some of the model predictions. Good agreement is found for the global burden and the annually averaged latitudinal gradient in the southern hemisphere and the tropics. A detailed comparison of the seasonal cycles of H_2 in surface air indicates that the use of the net primary productivity to prescribe the seasonal and geographical pattern of soil uptake in the model leads to an underestimate of the deposition velocity during winter and spring over the continents in the northern hemisphere. *INDEX TERMS:* 0322 Atmospheric Composition and Structure: Constituent sources and sinks; 0365 Atmospheric Composition and Structure: Troposphere—composition and chemistry; 0368 Atmospheric Composition and Structure: Troposphere—constituent transport and chemistry; *KEYWORDS:* molecular hydrogen

Citation: Hauglustaine, D. A., and D. H. Ehhalt, A three-dimensional model of molecular hydrogen in the troposphere, *J. Geophys. Res.*, *107*(D17), 4330, doi:10.1029/2001JD001156, 2002.

1. Introduction

[2] Molecular hydrogen, H_2, has an average tropospheric mixing ratio of about 530 ppbv [*Novelli et al.*, 1999]. It is thus the second most abundant oxidizable trace gas in the troposphere after methane, CH_4, with an average mixing ratio of 1745 in 1998 [*Dlugokencky et al.*, 1998]. Moreover, with about 40 Tmole/yr, H_2 has a large turnover in the troposphere, second only to that of carbon monoxide, CO, but as large as that of CH_4 in these molecular units [*Ehhalt*, 1999]. The presence of H_2 in the troposphere had been recognized for a long time - the first measurements being reported by *Paneth* [1937]. However its major sources and sinks were not identified before the early seventies [*Schmidt*, 1974]. H_2 is produced by the same processes as CO [*Ehhalt*, 1999]. Thus, most of its major sources are identical to those of CO, namely incomplete combustion of fossil fuel, biomass burning, and the atmospheric oxidation of hydrocarbons, notably of CH_4. The sinks are also similar: atmospheric oxidation initiated by the reaction with the hydroxyl radical, OH, and microbial uptake in soil, generally parameterized in models by a dry deposition velocity [*Schmidt*, 1974]. But, whereas CO is mostly destroyed by atmospheric oxidation, reaction of H_2 with OH is slow and

0148-0227/02/2001JD001156

tropospheric H_2 is removed predominantly by soil uptake. This is a unique feature among the oxidizable trace gases with the consequence that the sink strength for tropospheric H_2 is hemispherically highly asymetric, much larger in the northern hemisphere owing to the larger continental area. As a corollary the H_2 mixing ratios observed in the northern hemisphere are lower than those in the southern hemisphere [*Khalil and Rasmussen*, 1990; *Novelli et al.*, 1999; *Simmonds et al.*, 2000], despite the fact that most of the known H_2 sources are located in the northern hemisphere.

[3] Three-dimensional modeling of the tropospheric cycle of hydrogen is interesting, because it provides important constraints on the atmospheric cycles of methane, nonmethane hydrocarbons (NMHCs), and carbon monoxide. It is also interesting, because molecular hydrogen has been proposed as a future energy supply. Although H_2 is considered to have few environmental impacts, there are some which are worth studying: for instance, the impact on tropospheric hydroxyl radicals by an increase in the H_2 concentration, which in in turn provides indirect radiative forcings by changing CH_4, HCFC and HFC lifetimes as well as the photochemical production of ozone. An increase in H_2 would also increase the concentration of stratospheric water vapor.

[4] After a number of publications in the seventies, which laid the groundwork for our current knowledge about atmospheric H_2 (see *Warneck* [1988], for a summary of the early results) little attention was paid to that topic until quite recently, when *Novelli et al.* [1999], presented an extensive set of H_2 measurements from a globally distributed sampling network. These data for the first time provide a global overview over the latitudinal and seasonal distribution of H_2 at the Earth's surface. They warrant a three-dimensional analysis by a global Chemical-Transport Model, CTM, whereas the limited earlier tropospheric measurements and budgets of H_2 could be satisfactorily interpreted by one- to two-box models.

[5] In the following we use the MOZART model to simulate the global and seasonal distribution of H_2. The simulation is based on current estimates of the H_2 emissions and their geographical distribution. The dry deposition is allowed to vary geographically and seasonally; its mean global rate is scaled to values available in the literature. After a brief description of the model and its inputs, we present the results on the spatial and temporal distribution of tropospheric H_2. Obviously the model distributions provide a more complete coverage than the measurement data and they exhibit systematic longitudinal and vertical gradients which had not been captured by the existing measurements. They may, thus, guide the design of future measurement campaigns. As a test of our current understanding of the tropospheric H_2 cycle, we compare the modeled with the measured distributions. In particular we investigate the latitudinal gradients in the annually averaged H_2 mixing ratios and the dependence of the seasonal cycle on latitude. The agreements and disagreements found allow conclusions about the seasonal pattern of dry deposition.

2. Description of the Global Chemical-Transport Model

[6] MOZART (Model for OZone And Related chemical Tracers) is a three-dimensional CTM of the global troposphere described and evaluated by *Brasseur et al.* [1998] and *Hauglustaine et al.* [1998]. The model accounts for surface emissions of chemical compounds (N_2O, CH_4, NMHCs, CO, NO_x, CH_2O, and acetone), advective transport (using the semi-Lagrangian transport scheme of *Williamson and Rasch* [1989]), convective transport (using the formulation of *Hack* [1994]), diffusive exchanges in the boundary layer (based on the parameterization of *Holtslag and Boville* [1993]), chemical and photochemical reactions, wet deposition of 11 soluble species, and surface dry deposition. The chemical scheme (based on *Müller and Brasseur* [1995]) includes 140 chemical and photochemical reactions and considers the photochemical oxidation schemes of methane (CH_4), ethane (C_2H_6), propane (C_3H_8), ethylene (C_2H_4), propylene (C_3H_6), isoprene (C_5H_8), terpenes (as α-pinene, $C_{10}H_{16}$), and a lumped compound n-butane (C_4H_{10}) used as a surrogate for heavier hydrocarbons. The evolution of species is calculated with a numerical time step of 20 min for both chemistry and transport processes. The model is run with a horizontal resolution which is identical to that of CCM (triangular truncation at 42 waves, T42) corresponding to about 2.8 degrees in both latitude and longitude. In the vertical, the model uses hybrid sigma-pressure coordinates with 25 levels extending from the surface to the level of 3 mb. Dynamical and other physical variables needed to calculate the resolved advective transport as well as smaller-scale exchanges and wet scavenging are precalculated by the NCAR CCM (version 2, Ω0.5 library), and provided every 3 hours from preestablished history tapes.

Table 1. Annual and Global Budget of Molecular Hydrogen in the Troposphere Based on MOZART and Compared to Previous Estimates[a]

	SC87	W88	N99	E99	MOZART
Industrial Emissions	20	17	15	20	16
Biomass Burning	20	15	16	10	13
Oceans	4	4	3	3	5
Nitrogen Fixation	3	3	3	3	5
Photochemical production	40	50	40	35	31
Total source	87	89	77	71	70
Oxidation by OH	8	11	19	25	15
Soil uptake	90	78	56	40	55
Total sink	98	89	75	65	70
Burden (Tg-H_2)	...	163	155	150	136
Lifetime (yr)	...	1.9	2–3	2.3	1.94

[a] Units are in Tg-H_2/yr. SC87, *Seiler and Conrad* [1987]; W88, *Warneck* [1988]; N99, *Novelli et al.* [1999]; E99, *Ehhalt* [1999].

[7] Table 1 shows the global emissions of molecular hydrogen used in MOZART and compares them to some of the previous estimates on which the present numbers are based. The major sources of H_2 are similar to those of CO and result from incomplete combustion of fossil fuel and biomass burning. The geographical distribution of H_2 technological sources (oil, gas, and coal burning and other industrial activities) are introduced in MOZART on the basis of the CO emission inventory provided by EDGAR [*Olivier et al.*, 1996]. The global mean CO emission by fossil fuel and industrial processes totals 382 Tg-CO/yr. This source is scaled to provide an annual mean emission of 16 Tg-H_2/yr based on recent estimates (see Table 1). The H_2/CO ratio of 0.042 is in agreement with the range of measured values as discussed by *Novelli et al.* [1999]. No

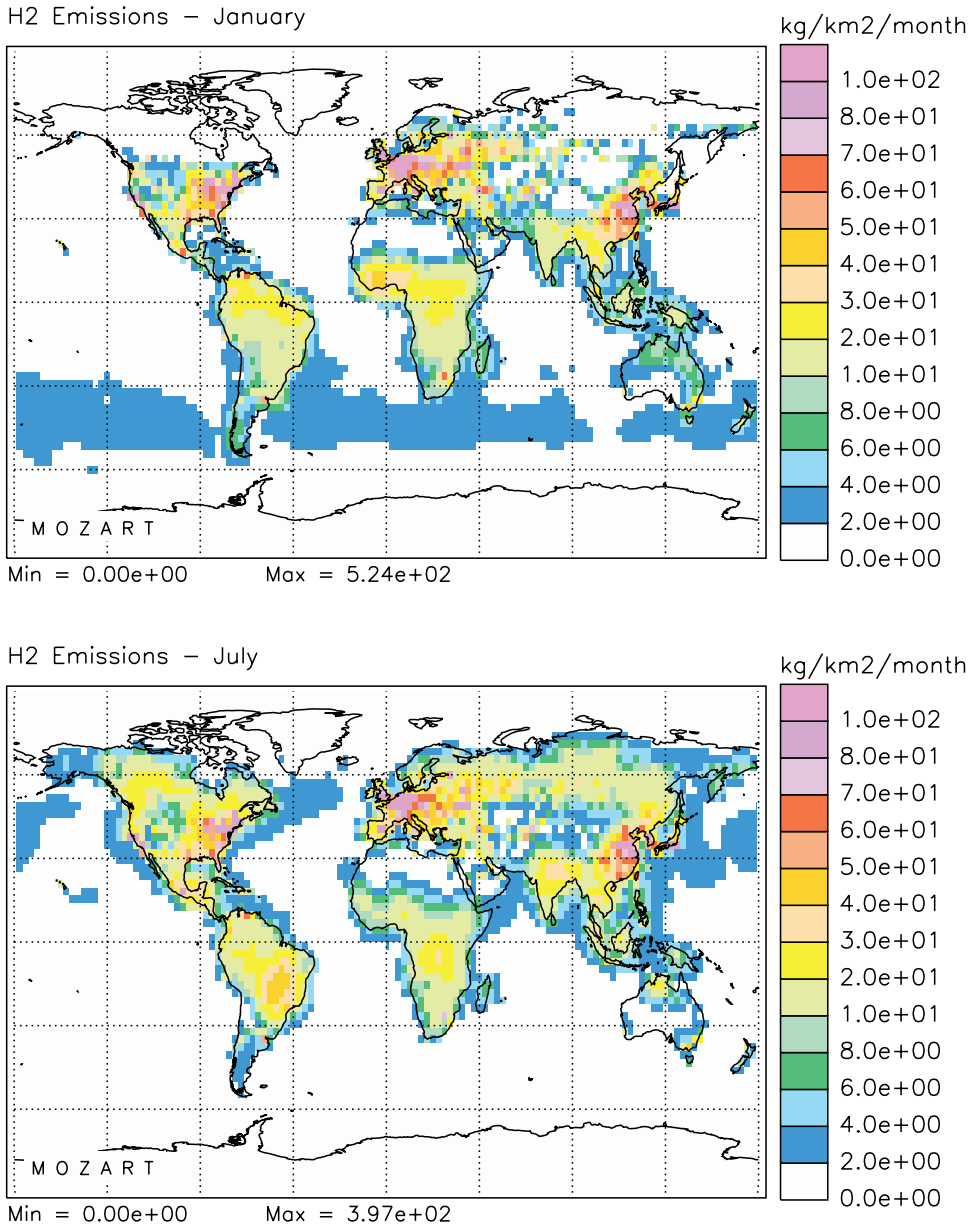

Figure 1. Monthly mean H_2 total surface emissions used in MOZART for January and July conditions ($kg/km^2/month$).

seasonal cycle of this source is considered in EDGAR and consequently in our model. Biomass burning is another major source of molecular hydrogen. The seasonal and geographical distribution of this emission is introduced in MOZART on the basis of the CO biomass burning emissions. In the case of CO, as described by *Brasseur et al.* [1998], the spatial and temporal distribution of biomass burned is taken from *Hao and Liu* [1994] in the tropics and from *Müller* [1992] in nontropical regions. The emission ratios of CO relative to CO_2 are taken from *Granier et al.* [1996] for each type of biomass fire except for savanna emissions, where the value suggested by *Hao et al.* [1996] is adopted. The global and annual emission of CO from biomass burning (including tropical and nontropical forest fires, savanna, fuelwood use, and agricultural waste burning) is 662 Tg-CO/yr. This source is scaled to provide a global molecular hydrogen emission of 13 Tg-H_2. The H_2/CO ratio of 0.02 for this source falls within the range of measured values as summarized by *Novelli et al.* [1999]. It should be noted that all biomass burning emissions are introduced in the model as surface fluxes in the lowest model level. All these source estimates are highly uncertain – up to an error of 50%. The emission of H_2 from the ocean and from biological nitrogen fixation is even more uncertain [*Conrad and Seiler*, 1980]. In this study, these two emissions are each rounded to 5 Tg on a global and annual mean basis which are in the range provided by the earlier estimates by *Schmidt* [1974] and *Conrad and Seiler* [1980]. The spatial and temporal distribution of ocean emissions is based on that of *Erickson and Taylor* [1992] for CO. For nitrogen fixation, the geographical and seasonal distribution of CO soil emissions given by *Müller* [1992]

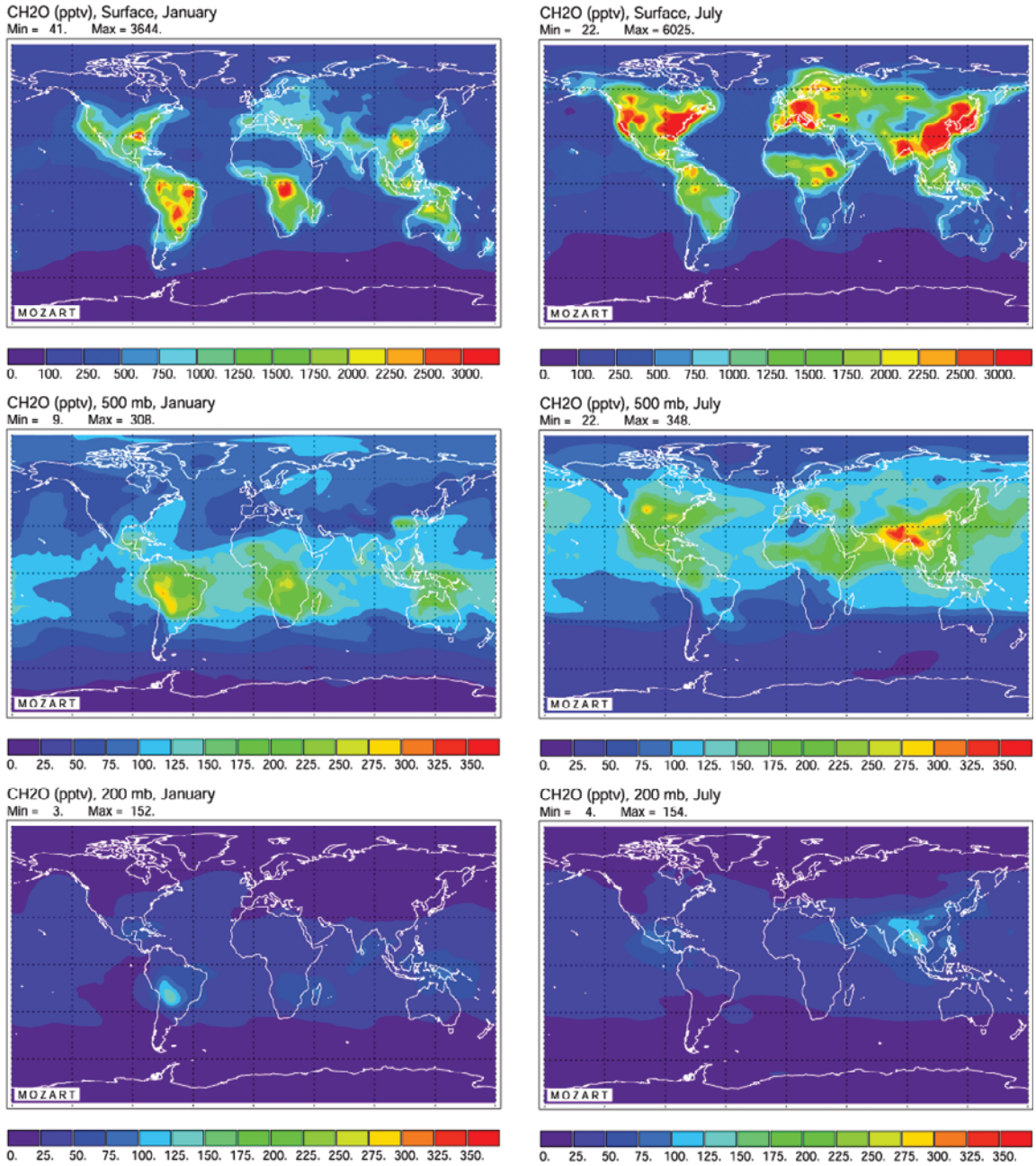

Figure 2. Distribution of CH_2O calculated at the surface, 500 mb, and 200 mb for January and July conditions (pptv).

are used and scaled accordingly. These global emission distributions are provided as monthly mean values and are linearly interpolated in time for each model time step.

[8] Figure 1 shows H_2 total emissions for January and July. During both seasons, the emissions of H_2 are large in Europe, the eastern United States, and eastern Asia, as a result of fossil fuel combustion, including automobiles. The contribution due to biomass burning is largest in the tropics, and its geographical distribution varies with season. Maximum biomass burning emissions are found north of the equator in Africa in January and south of the equator in Africa and southern America in July. Ocean emissions are also visible in marine high productivity regions.

[9] The photochemical production of H_2 arises mainly from the photolysis of formaldehyde. In MOZART, the distribution of formaldehyde is calculated accounting for the oxidation of CH_4 and NMHCs. The simulated distribution of CH_2O has been evaluated through comparison against available measurements by *Hauglustaine et al.* [1998]. A general agreement between model and measurements was reported in this previous work. Figure 2 shows the CH_2O distribution calculated at the surface, 500 mb and 200 mb for January and July conditions. Maximum mixing ratios of 2–6 ppbv are simulated at the surface over the continents in the northern hemisphere where photochemical production from hydrocarbon oxidation prevails (i.e., north-

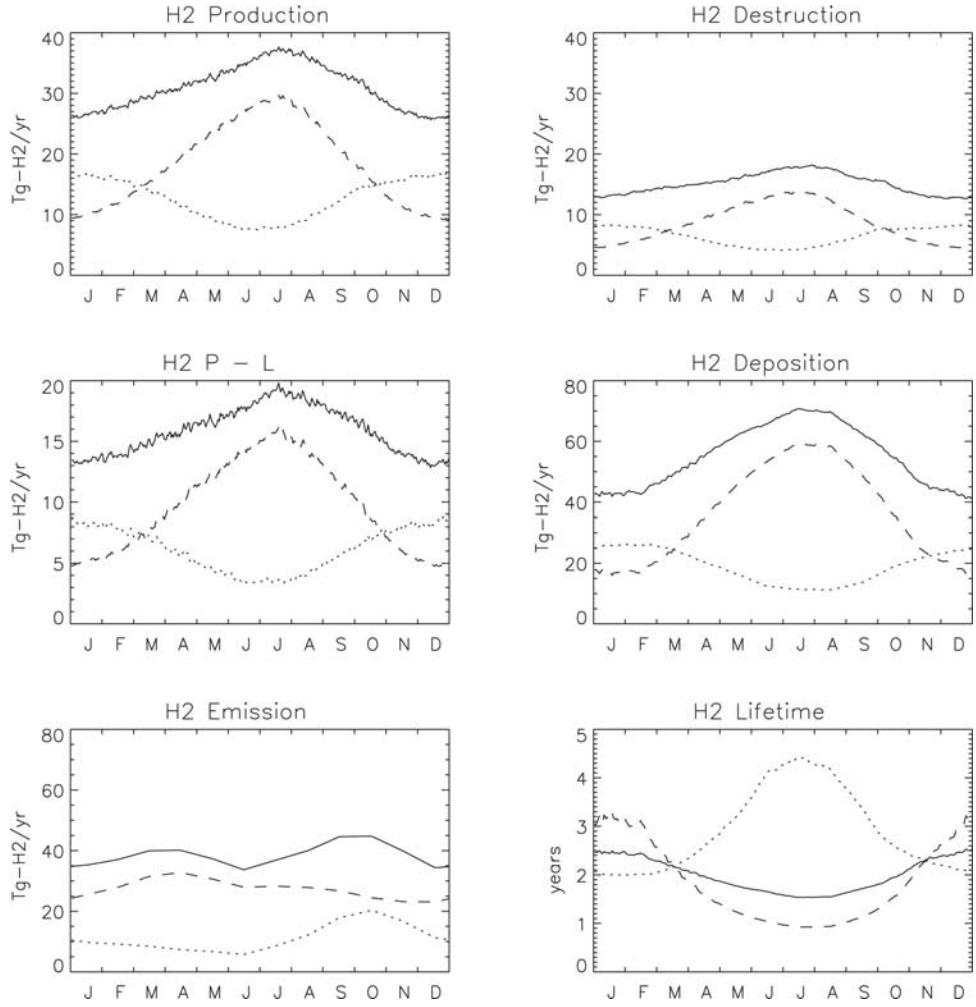

Figure 3. Seasonal variation of integrated H_2 photochemical production, destruction, and net production (Tg/yr), surface dry deposition, and surface emission (Tg/yr), and atmospheric lifetime (yr) calculated by the model. The northern hemisphere values are represented by the dashed line, southern hemisphere is the dotted line, and the solid line is the global integral.

ern United States, Western Europe, Southeast Asia). In the tropics, mixing ratios of 1–3 ppbv are predicted over biomass burning regions or where biogenic emissions of hydrocarbons are high (i.e, South America, Africa, Indonesia). Since the formaldehyde lifetime against oxidation by OH and photolysis is less than a day in summer, this species is moderately affected by transport processes. Over the ocean, the mixing ratios are generally in the range 0.1–0.5 ppbv. In the free troposphere (500 mb), maximum mixing ratios of 0.2–0.3 ppbv are calculated in convective regions as a result of rapid transport from the boundary layer. At this altitude, background mixing ratios are in the range 0.03–0.15 ppbv. In the upper troposphere, the mixing ratios are lower than 50 ppbv except over convective regions where it reaches 0.1–0.15 ppbv locally.

[10] As indicated by previous work [e.g., *Schmidt*, 1974; *Warneck*, 1988; *Ehhalt*, 1999; *Novelli et al.*, 1999], soil uptake is the largest loss process of H_2. This term is poorly defined and depends mainly on the microbial activity in the soil, the soil texture and moisture content which control the diffusion of H_2 to the active sites [*Conrad and Seiler*, 1985]. The latter induces a seasonal variation in the soil uptake of H_2 with lower rates during winter at northern midlatitudes. The uptake is often parameterized as a dry deposition at the surface. No information on the quantitative dependence of H_2 deposition on soil wetness and texture is currently available. For lack of a better alternative we used the Net Primary Productivity (NPP) to constrain the seasonal and geographical distribution of the dry deposition velocity (v_d), as proposed by *Müller* [1992] for CO and used by *Müller and Brasseur* [1995] and *Brasseur et al.* [1998]. A linear relationship between CO and H_2 deposition has been inferred by *Yonemura et al.* [2000] based on several data sets collected at various sites. In our study, both CO and H_2 deposition velocities are based on NPP and a constant ratio of 1.5 is assumed for $v_{d_{H_2}}/v_{d_{CO}}$ [*Hough*, 1991]. This ratio is in the range of deposition velocities measured over various soil types and reported by *Conrad and Seiler* [1980, 1985] and *Yonemura et al.* [2000]. The resulting H_2 deposition velocity is illustrated in Figure 2 for January and July conditions. The velocity ranges from very low values in winter over the continents in the northern hemisphere to

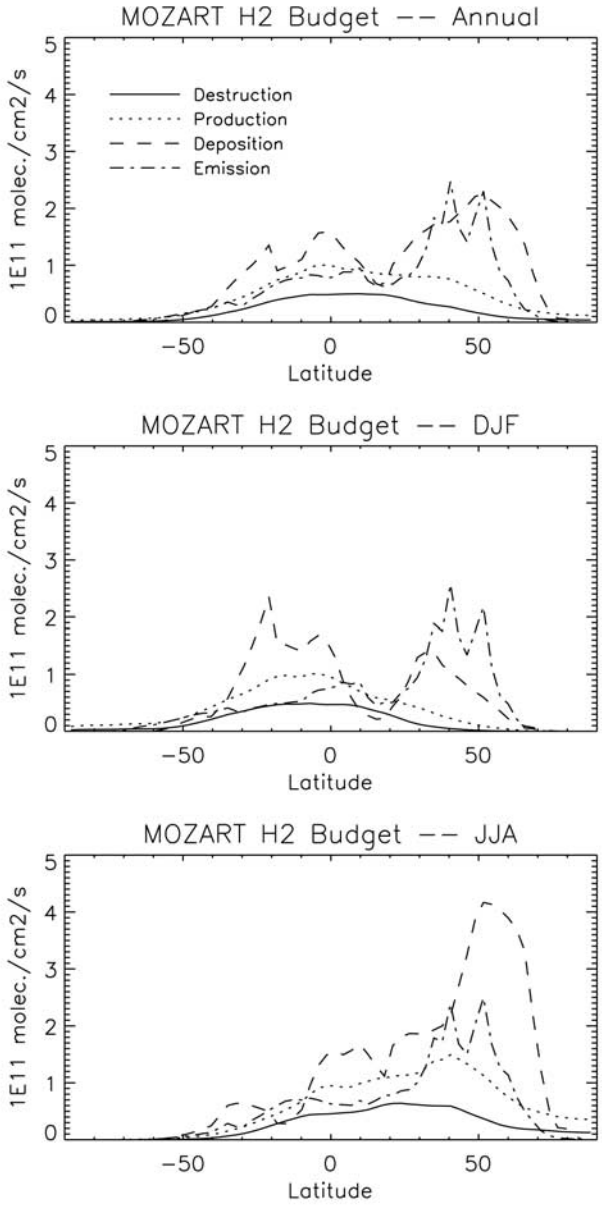

Figure 4. Latitudinal variation of H_2 photochemical production, destruction, surface emission, and surface deposition (10^{11} molecules/cm^2/s) calculated for annual mean, December–January–February (DJF), and June–July–August (JJA) conditions.

values of 0.06–0.1 cm/s during summer. A significant seasonal cycle is also derived for the tropics with peak values during the dry season reaching 0.06–0.09 cm/s. The deposition velocity averaged over continental areas is 0.025 cm/s in January and 0.036 cm/s in July.

3. Model Results

[11] Table 1 provides an estimate of the global budget of H_2 in the troposphere as calculated by MOZART. Figure 3 shows the seasonal cycle of the various budget components and Figure 4 their latitudinal distribution. The molecular hydrogen photochemical production through CH_2O photolysis totals 31 Tg on a global and annual mean basis. The production is characterized by a strong seasonal cycle and ranges from 25 Tg in January to 36 Tg in July (Figure 3). The production peaks in summer (when photorates are maximum) at northern midlatitudes (Figure 4) where CH_2O and OH concentrations are more important (Figure 5). This term accounts for about 45% of the molecular hydrogen total production (photochemical + emissions). Photochemical oxidation totals 15 Tg on the global scale and ranges from 13 Tg in January to 18 Tg in July. The net chemical source (production - loss) is 16 Tg on a global mean basis and peaks in summer (18 Tg) in the northern hemisphere. The H_2 loss is dominated by soil uptake. This term totals 55 Tg and accounts for about 80% of the loss processes. The soil uptake (parameterized as surface deposition) ranges from about 40 Tg in January to 70 Tg in July. As shown in Figure 4, this loss term is dominated by a tropical uptake during all seasons and by an large uptake by the continents in the northern hemisphere during summer. The calculated H_2 lifetime is 1.9 yr in annual mean. This value compares well with the estimates by *Warneck* [1988], *Novelli et al.* [1999], and *Ehhalt* [1999] which give 1.9 yr and 2.3 yr, respectively. The lifetime associated with oxidation by OH is calculated to be 9 years.

[12] Figure 6 shows the distribution of H_2 calculated at the surface, 500 mb and 200 mb for January and July conditions. Surface mixing ratios exhibit significant geographical and seasonal variations. In the northern hemisphere, maximum mixing ratios are predicted over source regions during winter and reach more than 650 ppbv over the northern United States, Europe, and Southeast Asia. During summer, when soil uptake is at maximum, mixing ratios lower than 450 ppbv are calculated over the continents. The important role played by soil uptake is also visible over forested regions in the tropics with mixing ratios as low as 425 ppbv over South America in January. Direct emissions and photochemical production associated with biomass burning activities are responsible for mixing ratios reaching 560 ppbv over Africa. This maximum follows the seasonal evolution of the dry season over the continent, peaking north of the equator in January and south of the equator in July. Maximum mixing ratios associated with biomass burning emissions are calculated in March in northern Africa and in October in southern Africa (not shown).

[13] More uniform mixing ratios are simulated in the free troposphere. At 500 and 200 mb, the H_2 mixing ratios are generally within the range 530–550 ppbv during all year. However, in the tropics where vigorous upward transport prevails, air depleted in H2 by soil uptake is rapidly lifted up to higher altitudes. Local minima of 510–520 ppbv are calculated at 500 and 200 mb over southern America and Africa in January and over Southeast Asia in July. Large scale meridional transport away from these regions featuring plumes with lower H_2 levels is also visible at these altitudes.

[14] More insight into the seasonal cyle of H_2 in the boundary layer is provided by Figure 7 which illustrates the maximum amplitude of the annual cycle (difference between the local maximum and the local minimum during the course of the year calculated on the basis of 24h averaged mixing ratios and expressed relative to the annual

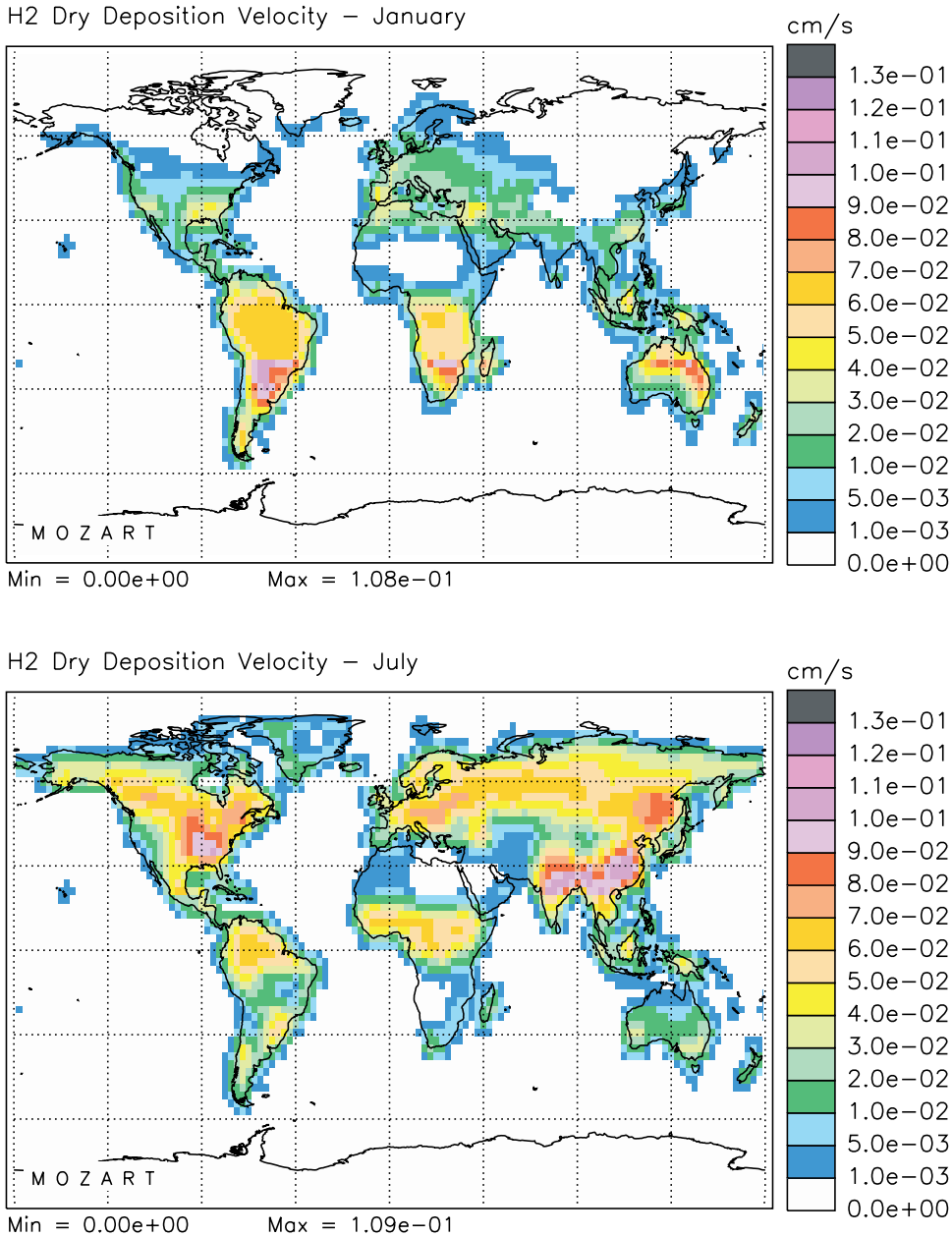

Figure 5. Monthly mean H_2 surface dry deposition velocity (cm/s) considered in MOZART for January and July conditions.

mean in %). Over the continents in the northern hemisphere, the annual cycle reaches an amplitude of more than 30% over Siberia where a strong soil uptake is predicted during summer. At midlatitudes, over the continents, an amplitude of 10–20% is simulated. The seasonal cycle shows secondary maxima of 20–30% over South America and Africa where uptake is also large and where biomass burning emissions contribute to direct and indirect emissions of molecular hydrogen.

[15] Figure 8 provides another perspective on the global distribution of H_2 in the atmosphere and shows the zonal-mean mixing ratio for January and July conditions. In January, the zonal mean mixing ratio is in the range 540–560 ppbv in the troposphere. Values in the 530–540 ppbv range are calculated as a result of surface uptake in the tropics and subsequent upward transport, as discussed earlier. In July, due to a larger surface uptake over the continents, minimum mixing ratios of 500 ppbv are simulated in the 50N–70N degrees latitude band. As a result, in these regions, significant vertical gradients are predicted during summer. A rather uniform distribution of about 540 ppbv is simulated elsewhere in the troposphere.

[16] Above the tropopause where the H_2 lifetime becomes much longer, the calculated mixing ratios increase with height. At 20 km the mixing ratio reaches more than 590 ppbv. Please note that in this version of the model we do not consider an explicit stratospheric chemistry. Therefore, the reactions of H_2 with Cl which could play a role in this region is not considered. We note, however, that the simulated stratospheric increase is consistent with the mid-

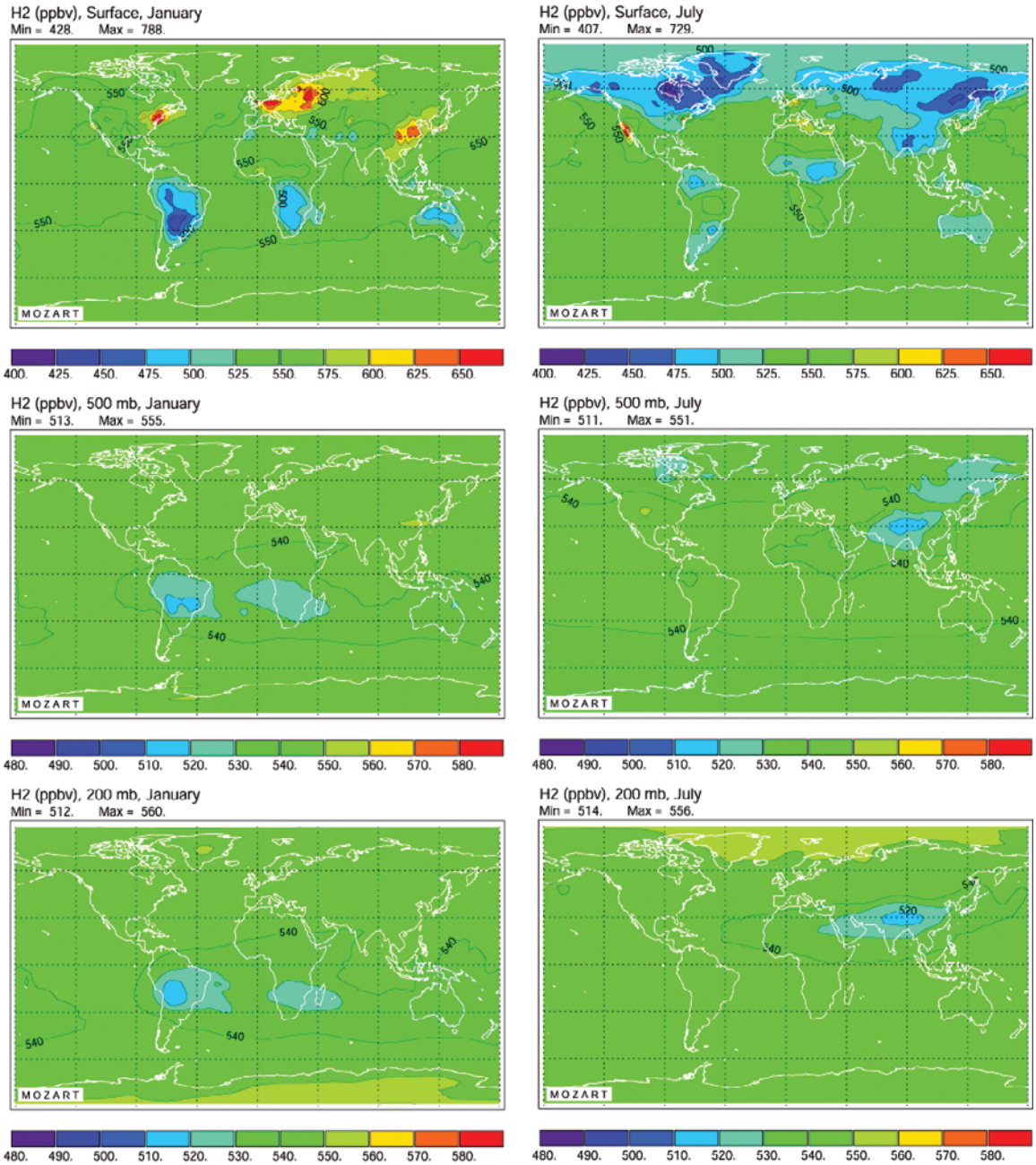

Figure 6. Distribution of H_2 calculated at the surface, 500 mb, and 200 mb for January and July conditions (ppbv).

stratospheric maximum measured by *Ehhalt et al.* [1977] at about 27 km.

4. Comparison With Measurements and Discussion

[17] Some of the seasonal and zonal patterns in the H_2 mixing ratio predicted by the model can be tested against experimental observations. For that comparison we rely on the data from the CMDL network of surface stations [*Novelli et al.*, 1999], because they provide the most complete global coverage. Other data are available in the literature [*Simmonds et al.*, 2000; *Francey et al.*, 1998; *Khalil and Rasmussen*, 1990]. However, these measurements usually come from a small subset of the stations covered by the CMDL network, and thus offer little additional information. They point, however, to differences in calibration between the various laboratories. Whereas *Novelli et al.* [1999] report a globally and annually averaged mixing ratio of (531 ± 6) ppbv for 1991 to 1996, *Khalil and Rasmussen* [1990] reported a value of 515 ppbv for the late 1980s, and *Simmonds et al.* [2000] estimate a "global" average (based upon 2 points, Mace Head and Cape Grim) of 512 ppbv for January 1996. The difference between the data from *Novelli et al.* [1999] and the other measurements cannot be explained by the trends reported for global H_2,

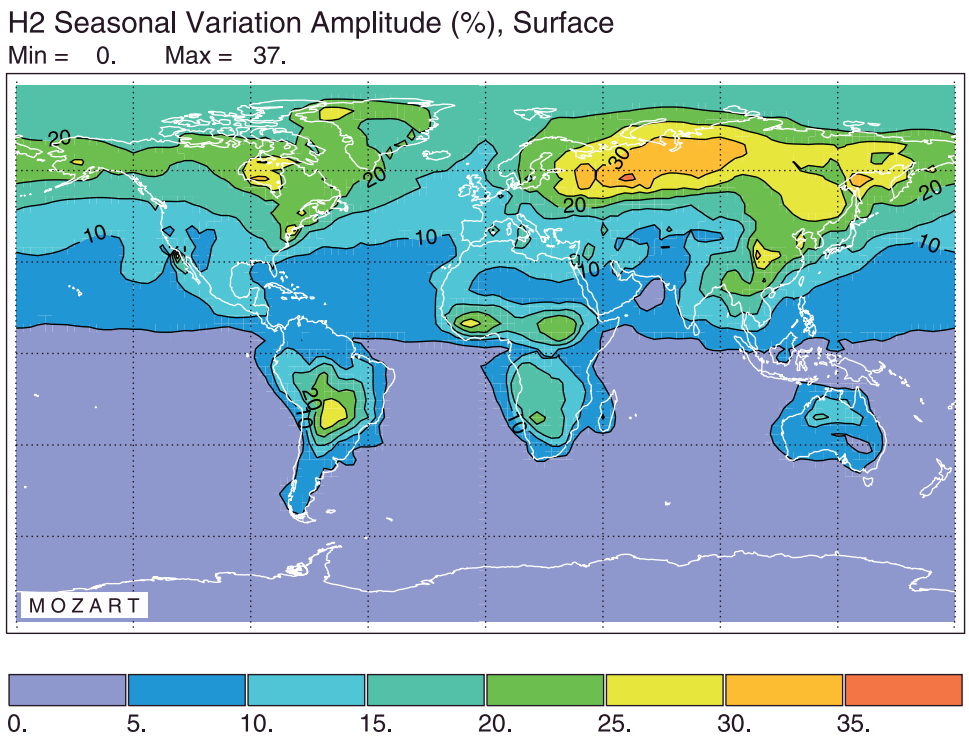

Figure 7. Seasonal cycle amplitude of H_2 surface mixing ratio (%). The amplitude is calculated as the difference between the local maximum and the local minimum during the year relative the local annual mean.

because they are small: $-(2.3 \pm 0.1)$ ppbv/yr between 1991 and 1996 according to *Novelli et al.* [1999], or $+(1.2 \pm 0.8)$ ppbv/yr between 1994 and 1999 according to *Simmonds et al.* [2000]. In comparison, the annual mean H_2 mixing ratio obtained by the model, when averaging over the grid boxes where the CMDL stations are located, is 540 ppbv. Considering the uncertainties in the model input the agreement with any of the experimental global averages is quite satisfactory and quite good with the CMDL data. It demonstrates that the model reproduces the tropospheric burden of H_2, B, reasonably well. Since $B = \tau \times S$, where τ is the tropospheric lifetime and S the global source strength of H_2, the model also reproduces this product reasonably well, but not necessarily the absolute magnitude of each of its factors.

[18] Discrepancies between model and measurements begin to emerge, when we consider distributions, such as the mean latitudinal gradient (Figure 9). Although model results and measurements agree in the southern hemisphere and the tropics, they display marked differences in the northern hemisphere. These differences increase with increasing latitude. At 80N latitude the difference between model and measurement data reaches about +50 ppbv. Such a tendency, although much weaker, is actually also present in the southern hemisphere south of 30S latitude. Around 45N latitude there is appreciable scatter in both the model and measurement data. This is caused by continental stations, which cluster around that latitude, and which have a tendency towards higher values in the model, but towards lower values in the measurements. For example, the two lowest values measured at this latitude were observed at Utah and Mongolia, the two highest model values were predicted for the stations in Hungary and Romania. Stations along the oceanic coast lines conform more closely to the respective averages.

[19] The fact that the difference between model results and measurement data increases with latitude in the northern hemisphere suggests that the balance between sources and sinks at higher latitudes is not correctly simulated. This could be due to too large source terms, to too small sink terms, or to both. We note, however, that the OH concentration in the model is fairly realistic as evidenced by the model calculated lifetime of CH_4 against removal by reaction with OH, which is 9.1 yr, and compares favorably with the 9.6 yr for that lifetime derived empirically [*Prinn et al.*, 1995]. Thus, if sinks are implicated, the difference would point to a too small soil uptake of H_2 in the model.

[20] Seasonal variations differ as well. Figure 10 shows the seasonal variation of the globally averaged H_2 mixing ratio. Clearly both, measured and modeled globally averaged H_2 exhibit a seasonal variation. But with a peak to peak amplitude of 23 ppbv the measured seasonal variation is only about one half of that modeled, which has a peak to peak amplitude of 47 ppbv. In addition the phase of the measured seasonal variation is delayed by about one month with respect to the modeled one. Since measured and modeled value agree around September, the time of the minimum, the differences become largest during March, the month when the modeled seasonal variation has its maximum. The seasonal variation in the modeled global H_2 can be explained with the help of Figure 3 above, which presented the seasonal variations in the major global source and sink terms in the model. It shows that atmospheric chemistry, i.e. H_2 generation from CH_4 and NMHC oxida-

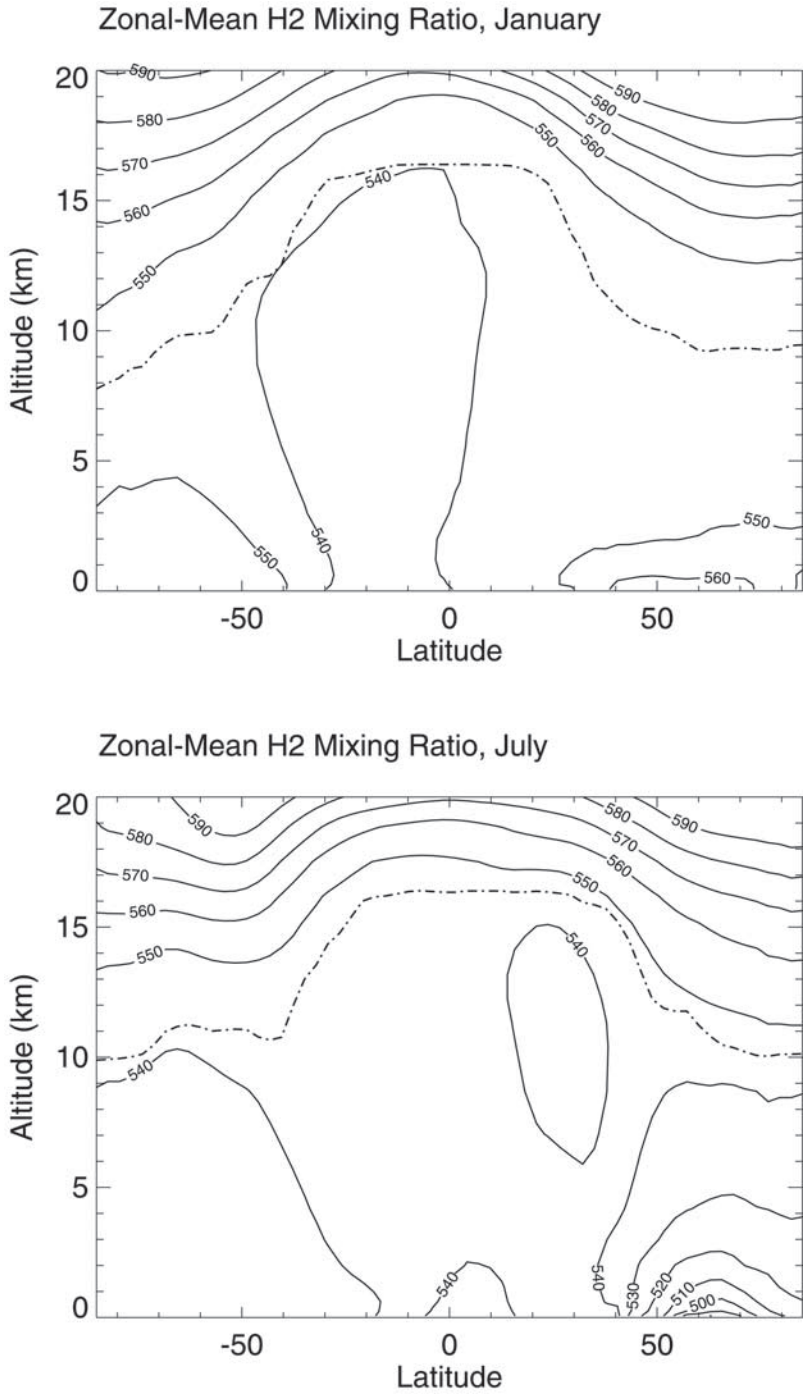

Figure 8. Zonally averaged H_2 mixing ratio (ppbv) cross sections calculated for January and July conditions. Dashed line indicates model tropopause.

tion minus H_2 oxidation by OH, results in a global net production of H_2 throughout the year with a maximum in July and August. This H_2 net production superimposes on the much larger surface emissions to a total with a weak semiannual modulation, since these emissions have two seasonal maxima, one in March, the other in September, caused by the different phase of biomass burning in the northern and southern hemisphere respectively. In contrast, global dry deposition has a strong seasonal variation with a single maximum in July and a minimum in December. Thus the seasonal variation in the modeled global H_2 mixing ratio is a result of the seasonal variation in the global dry deposition of H_2, which in turn is dominated by the signature of the dry deposition in the northern hemisphere (see Figure 3). The positions of the maximum and minimum in the annual variation of global H_2 are determined by the crossover points between the annual profile for dry deposition and that of the total net production as defined above.

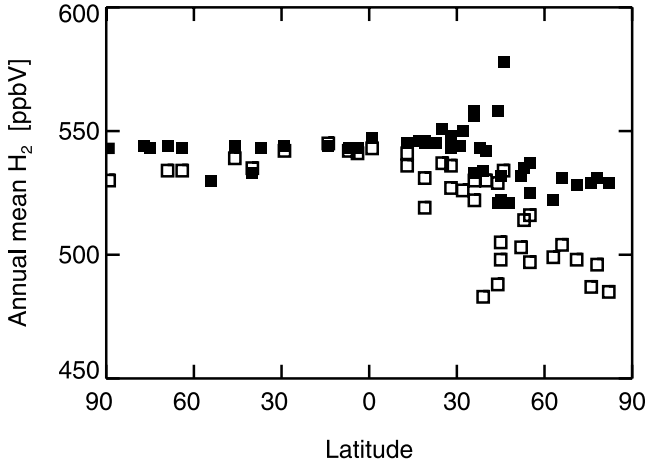

Figure 9. Latitudinal distribution of the annually averaged H_2 mixing ratio at the Earth's surface (ppbv). The measured values at the CMDL stations are indicated by the open squares. They represent averages over the time period 1992–1996 and include all stations for which that average could be calculated. The model values are indicated by the full squares. They represent the annual average in the model grid boxes where the CMDL stations are located and include also the few CMDL locations that provided data outside that time period.

The fact that the measured, globally averaged H_2 mixing ratio also shows a seasonal variation, indicates that the global dry deposition indeed varies with season, but possibly with a different amplitude and a slightly different phase than assumed in the model. In turn, the seasonal pattern in the difference to the modeled seasonal variation provides an additional clue to its cause.

[21] To check where the difference in the seasonal variation of global H_2 arises, Figure 11 compares modeled and measured seasonal variations at different latitudes. In the southern hemisphere and the tropics the seasonal variation is weak, and modeled and measured variations agree. In contrast, the seasonal amplitude in the northern hemisphere becomes large and increases with latitude. At the same time, the modeled and measured variations diverge at least between the tropics and midlatitudes. The divergence is similar in form for all stations in the northern hemisphere, although it is particularly large in amplitude for the two continental stations, Utah and Mongolia. The differences occur mainly during winter and spring; during summertime modeled and measured data agree - just like the globally averaged seasonal variation (Figure 10).

[22] Figure 12 develops the differences between modeled and measured seasonal variation in a more systematic way; it compares phase and amplitude of modeled and measured seasonal variations as a function of latitude. In many ways, model results and measurements appear to be in reasonable agreement. The exception is the latitudinal pattern in the seasonal maximum in the northern hemisphere, where the model predicts mixing ratios above 550 ppbv and slightly increasing with latitude, whereas the measured seasonal maxima generally fall below 550 ppbv and decrease with increasing latitude (the few outliers are mainly from continental stations). As a result, the spring maxima of the modeled and measured seasonal variation, and thus the seasonal variations themselves, increasingly diverge with higher latitudes.

[23] Figure 12, together with Figures 9 and 11, characterizes the geographical pattern of the difference between measured and modeled seasonal variation. The salient features are as follows: (1) The difference is a phenomenon of the northern hemisphere, where it is ubiquitous; it is quite small in the southern hemisphere (Figures 11 and 12). (2) The differences are stronger in the interior of the continents than along the coast lines (Figure 11). (3) The difference increases with northern latitudes, i.e. with the fraction of latitude covered by land. In other words it has a geographical pattern compatible with that of dry deposition. Its period of one year is also compatible with that of dry deposition (see Figure 3).

[24] As a consequence, much of the difference between the modeled and measured geographical and temporal distribution of H_2 can be removed by a simple and relatively small adjustment of the model's dry deposition: an increase of about 15% of the dry deposition in the northern hemisphere during the winter half year would go a long way in bringing model results in quite good agreement with the measurements for all of the dependencies we have discussed. Such a correction is well within the uncertainties of dry deposition which is the largest but most poorly characterized term among sources and sinks.

[25] An explanation based on other sinks and sources would require relatively larger and less plausible, or more complex adjustments. For instance, the loss of H_2 due to reaction with OH has a compatible seasonal variation, but is much more evenly distributed between the hemispheres. It is also more uniform in longitude. Moreover, it is a much

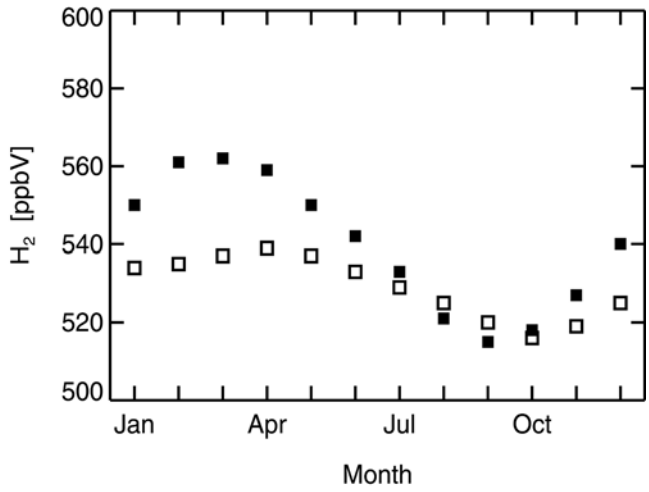

Figure 10. Seasonal variation of the globally averaged H_2 mixing ratio. The values derived from measurements are indicated by the open squares; they represent monthly averages over the CMDL stations during the year 1996 [cf. *Novelli et al.*, 1999, Figure 6]. The model values are indicated by the full squares; they represent the monthly averages over the model grid boxes where the CMDL stations are located.

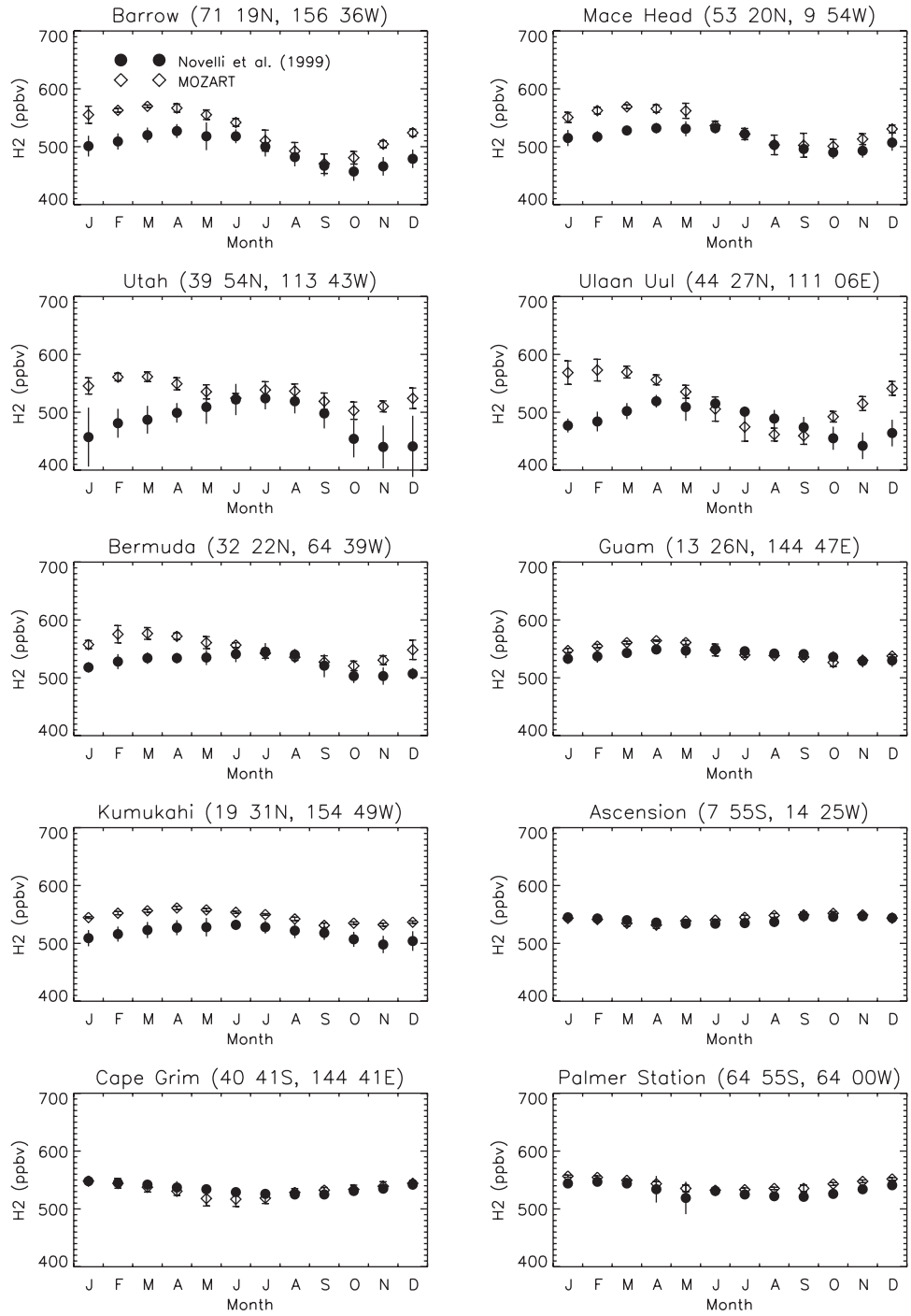

Figure 11. Modeled (diamonds) and measured (dots) seasonal variations in the H_2 mixing ratio at the Earth's surface for a number of stations at different latitudes. The stations Utah and Ulaan Uul are continental; all others are coastal or insular. The error bars indicate the mean standard deviation. Measurements are from *Novelli et al.* [1999].

smaller term. To generate the same integrated loss during winter as a 15% increase in dry deposition, about 1.5 Tg H_2/yr, would require an increase of >100% in the wintertime loss due to OH. This seems quite implausible. By the same token atmospheric net production of H_2, the difference between the production of H_2 from CH_2O photolysis and destruction of H_2 by OH, has a compatible seasonality, but is more evenly distributed between the hemispheres (Figure 4). It would require a decrease of 45% in the winter northern hemisphere to cause the same effect as a 15% increase in dry deposition. This appears again less plausible given the better state of knowledge in atmospheric chemistry than in dry deposition. Total surface emissions have a compatible latitudinal distribution, but exhibit only a small seasonal

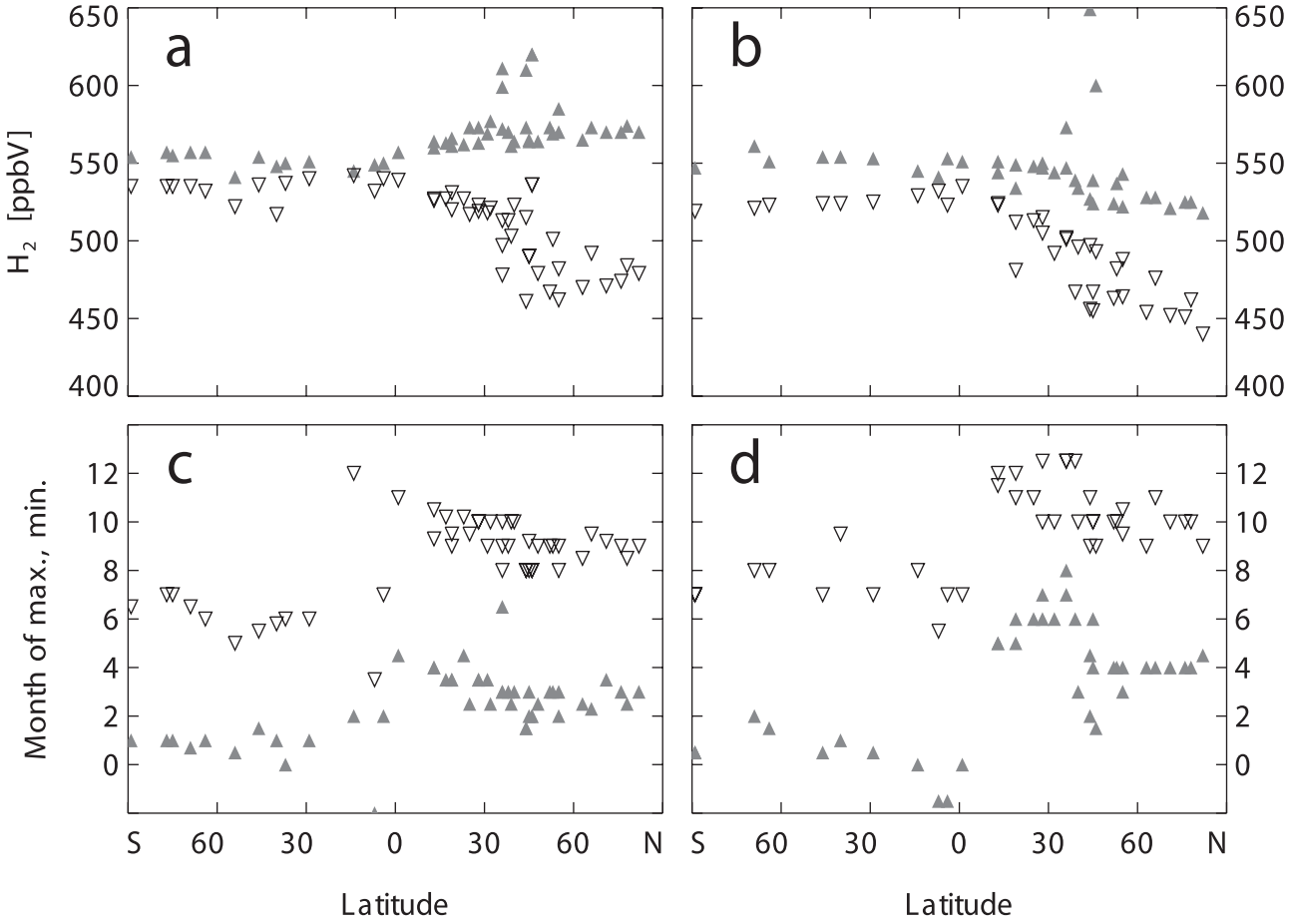

Figure 12. Latitudinal dependence of the maximum and minimum amplitudes (panels (a),(b)), and their phases (panels (c),(d)) in the modeled and measured seasonal variations of the H_2 mixing ratio at the Earth's surface. Upward pointing triangles refer to maxima, downward pointing triangles to minima. The measured values (panels (b),(d)) are taken from the monthly means obtained at the stations of the CMDL network in 1996 [*Novelli et al.*, 1999]. The modeled values (panels (a),(c)) are the monthly means from the model grid boxes where the CMDL stations are located.

variation in the northern hemisphere, about 30% peak to peak instead of a factor of 3 as for dry deposition (see Figure 3). They would need an increase in seasonal modulation with about 12% lower emission rates in the northern hemisphere during winter to account for the difference between modeled and measured seasonal variation in H_2. At a first glance this does not seem implausible. However, surface emissions are made up of four components, each with its own seasonal variation. Of these, biomass burning and industrial emissions are by far the dominating terms. They have well defined geographical and seasonal patterns. Biomass burning peaking in the tropics has an incompatible geographical distribution. Moreover, it is already very small in the extra tropical winter northern hemisphere. Thus an uniform adjustment in the winter northern hemisphere would not explain the seasonal and geographical pattern observed in the difference. In any case the required decrease during northern hemisphere winter would amount to at least 45%, if the change was assigned to biomass burning alone. Industrial emissions of H_2 in the model do not vary with season, and there is no evidence in the published emission rates of H_2 or CO that they should. They have, however, a compatible latitudinal distribution. Their needed adjustment would be −20% in the winter northern hemisphere. This is not very plausible. If anything, fossil fuel and biofuel consumption peaks during winter in the northern hemisphere, mostly due to an increase in fuel consumption for heating [*Rotty*, 1987; *Liousse et al.*, 1996]. Thus the corresponding emissions of H_2 would have to be increased rather than decreased during winter. Of course, a combination of changes in the source terms could conceivably explain the difference between modeled and measured seasonal variation. But this would need tuning of quite a few parameters both in the spatial and temporal distribution of the various sources. This does not appear plausible, when a much simpler solution, namely upward adjustment of dry deposition is at hand.

[26] So far we have not introduced that modification, because there is insufficient information on the seasonal cycle of H_2 dry deposition in the literature to verify the present conclusions. Moreover, there is no algorithm to define the dependence of H_2 dry deposition on the environmental parameters that appear to control it, such as soil moisture, or porosity, a lack which necessitated our choice

of NPP as a measure for the geographical and seasonal variation in the dry deposition.

[27] To our knowledge, there are only three studies which measured the dry deposition velocity of H_2 on soil over the period of a full year. The first study measured the uptake of H_2 by grass and clover fields at Mainz, Germany [*Conrad and Seiler*, 1980], the second that by arable land (parabraunerde) close to Jülich, Germany [*Förstel*, 1986], and the third that on arable land and forest soil near Tsukuba, Japan [*Yonemura et al.*, 2000]. Only the first study measured a seasonal variation of the dry deposition velocity, v_d, which approximately agrees with that in the model. The others differ and they differ among each other as well. In the first study v_d reached a maximum in summer averaging 0.07 cm/s; in winter, from December through March, v_d was a factor of 3 lower. The second study found a maximum v_d from April to September with values varying from 0.01 to 0.08 cm/s; much lower values of 0.001 cm/s or less were observed from October through March. The forest soil in the third study showed no systematic seasonal variation, but fluctuated randomly by about 0.01 cm/s around a mean v_d of 0.07 cm/s throughout the year. On arable land the seasonal variation had two maxima, one in February and March, the other in July and August, both with a v_d of 0.07 cm/s. Lower and highly fluctuating values prevailed in between averaging 0.02 cm/s. The second and third study noted a strong anticorrelation of v_d with the soil moisture content in arable fields and found a somewhat weaker anticorrelation for forest soils. This control of v_d by soil moisture, clogging the pores and impeding the diffusion of H_2 in the top soil layers, had been noted earlier (see *Schuler and Conrad* [1991]). Given the high variability observed in v_d and its seasonal variation, and the incomplete understanding of its control parameters, a reliable parameterization of H_2 dry deposition on a global scale has so far not been attempted and is probably not yet feasible.

[28] A closer inspection reveals other interesting features in Figure 12. For the present purpose, the most important are as follows: a latitudinal dependence in the phase of the seasonal variation which shows similar patterns in both modeled and measured data. Maxima and minima are separated by about 6 months in both hemispheres and data sets. But generally the measured extrema lag by about one month behind the modeled ones in both hemispheres. This indicates that dry deposition in the model may also need a temporal adjustment. The phase of the seasonal variation shows a steep transition - close to the equator in the model, between 15N and the equator for the measured data - from the northern to the southern mode. On average the phase difference between northern and southern hemispheric seasonal variation is only about 3 months rather than the 6 months observed for CH_4 or CO in both model and measurements. The fact that the model captures the anomalous phase in the southern hemisphere means it also provides an explanation for it. Since the latitudinal gradient in the H_2 mixing ratio of the southern hemisphere is small, most of its seasonal variation must be driven by the interplay of the regional sinks and sources. Figure 3 shows that in contrast to the global atmosphere (and the northern hemisphere) the surface emissions in the southern hemisphere - being dominated by biomass burning - have a strong seasonal variation with a single maximum in October. That seasonal variation is only slightly smoothed by the superposition of the relatively weak net atmospheric H_2 production which maximizes in December. Thus in the southern hemisphere net total production and dry deposition, both, exhibit a strong approximately sinusoidal seasonal variation with a phase shift of about 2 months between each other. The crossover points between these two curves, which define the annual extrema in the H_2 mixing ratio are in June (for the minimum) and in December (for the maximum) in good agreement with the modeled seasonal variation in the southern hemisphere (Figures 11 and 12). Thus the observed anomalous seasonal variation of H_2 is essentially a result of the specific seasonality in biomass burning and dry deposition in the southern hemisphere.

[29] This comparison of model and measured data allows to improve mainly the temporal and geographical distribution of the sources and sinks of H_2 in the model, since both leave a clear signature on the tropospheric distribution of H_2. It is of lesser value in testing the absolute strengths of the H_2 sources and sinks. In the case of H_2 the major contributors to both reside at the Earth's surface and their strengths are external and independent inputs to the model. Increasing the global strengths of the surface sinks and sources in a consistent manner would introduce little change in the tropospheric distribution of H_2. This makes it difficult to optimize for the respective strengths based solely on the differences between measured and modeled distributions of tropospheric H_2. On the other hand, the present model results on the global H_2 distribution appear quite reasonable. They capture the essence, and with the correction indicated will also capture the details of the measured spatial and temporal distribution of H_2 quite well. The adopted strengths of the surface source and sinks are well within the range of the current estimates based on emission and deposition estimates. The model should thus represent a good integration of the current knowledge in the cycle of tropospheric H_2.

5. Conclusions

[30] In this study, a global chemistry-transport model is used to simulate the distribution and budget of molecular hydrogen in the troposphere. The surface emissions of H_2 associated with technological sources, biomass burning, nitrogen fixation in soils, and oceanic activity are introduced in the model with a spatial and temporal distribution based on CO emissions. Photochemical production from formaldehyde photolysis is calculated including methane, as well as anthropogenic and biogenic nonmethane hydrocarbons. H_2 loss processes include atmospheric oxidation by OH in the atmosphere and soil uptake, which is parameterized using the Net Primary Productivity as a proxy for dry deposition velocity.

[31] Photochemical production represents about 45% of the total source of H_2, direct surface emissions contributing the remaining. This photochemical production peaks in the boundary layer over northern hemisphere continents in summer when CH_2O concentrations and photolysis are maximum. Soil uptake represents the major loss process, contributing 80% to H_2 destruction. The overall H_2 lifetime in the atmosphere is 1.9 years.

[32] H_2 is rather well-mixed in the free troposphere. However, its distribution exhibits a significant seasonal cycle in the lower troposphere where soil uptake dominates. This loss process shows a strong temporal variability and is maximum over the northern hemisphere landmass during summer. In these regions, H_2 mixing ratio varies by more than 30% between the winter maximum and the summer minimum. This feature induces strong vertical gradients over landmasses during summer and is also responsible for the unique behavior of H_2 in the atmosphere. Despite the fact that most sources in the model are associated with anthropogenic activities in the northern hemisphere, modeled H_2 levels are higher in the southern hemisphere.

[33] Our results stress the important role played by the tropics in the budget of H_2. In these regions a strong seasonal cycle is also predicted due to the annual variation in both biomass burning emissions and soil uptake. Furthermore, due to strong upward transport, the seasonal cycle in the tropics is not confined to the lower troposphere but propagates up to the mid and upper troposphere. Air masses depleted in H_2 by soil uptake are rapidly transported in the free troposphere leading to minimum mixing ratios over Africa and South America up to 200 mb.

[34] Comparison of the modeled H_2 mixing ratios against measurements from the CMDL global sampling network shows a general good agreement in the southern hemisphere and in the tropics. Discrepancies emerge in the northern hemisphere where the model overestimates by 50% the amplitude of the seasonal signal. In addition, in these regions the modeled maxima occur one month earlier than the observed ones. These differences point to an imprecise treatment of dry deposition leading in particular to a too small uptake during winter and spring over the continents in the northern hemisphere.

[35] In this first attempt to simulate the global three-dimensional budget of H_2, the absence of an algorithm to define the dependence of H_2 dry deposition on environmental parameters leads us to use the NPP to constrain the seasonal and geographical distribution of soil uptake. This feature appears to be the main limitation to fully capture the essence of the spatial and temporal distribution of H_2 in the model. A more complete understanding of the soil uptake and its control parameters based on measurements on a variety of sites and over the period of a full year is clearly needed. The model should then provide a better integration of our current knowledge in the cycle of troposphere H_2.

[36] **Acknowledgments.** We gratefully thank P. Novelli and the NOAA/CMDL for providing the molecular hydrogen measurements. Thanks to L. Emmons for help in data processing. Helpful discussions, and comments on this work by G. Brasseur were particularly appreciated. Part of this work was carried out at the National Center for Atmospheric Research (NCAR), Boulder, Colorado. The National Center for Atmospheric Reasearch is sponsored by the National Science Foundation.

References

Brasseur, G. P., D. A. Hauglustaine, S. Walters, P. J. Rasch, J.-F. Müller, C. Granier, and X. X. Tie, MOZART, a global chemical transport model for ozone and related chemical tracers, 1, Model description, *J. Geophys. Res.*, *103*, 28,265–28,289, 1998.

Conrad, R., and W. Seiler, Contribution of hydrogen production by biological nitrogen fixation to the global hydrogen budget, *J. Geophys. Res.*, *85*, 5493–5498, 1980.

Conrad, R., and W. Seiler, Influence of temperature, moisture, and organic carbon on the flux of H_2 and CO between soil and atmosphere: Field studies in subtropical regions, *J. Geophys. Res.*, *90*, 5699–5709, 1985.

Dlugokencky, E. J., K. A. Masarie, P. M. Lang, and P. P. Tans, Continuing decline in the growth rate of the atmospheric methane burden, *Nature*, *393*, 447–450, 1998.

Ehhalt, D. H., Gas phase chemistry of the troposphere, in *Global Aspects of Atmospheric Chemistry, Topics Phys. Chem.*, vol. 6, edited by R. Zellner, pp. 21–109, Springer-Verlag, New York, 1999.

Ehhalt, D. H., U. Schmidt, and L. E. Heidt, Vertical profiles of molecular hydrogen in the troposphere and stratosphere, *J. Geophys. Res.*, *82*, 5907–5911, 1977.

Erickson, D. J., III, and J. A. Taylor, 3-D tropospheric CO modeling: The possible influence of the ocean, *Geophys. Res. Lett.*, *19*, 1955–1958, 1992.

Förstel, H., Uptake of elementary tritium by the soil *Radioprot*, *Dosimetry*, *16*, 75–81, 1986.

Francey, R. J., et al., Atmospheric carbon dioxide and its stable isotope ratios, methane, carbon monoxide, nitrous oxide, and hydrogen from Shetland Isles, *Atmos. Environ.*, *32*, 3331–3338, 1998.

Granier, C., W. M. Hao, G. Brasseur, and J.-F. Müller, Land use practices and biomass burning: Impact on the chemical composition of the atmosphere, in *Biomass Burning and Global Change*, edited by J. S. Levine, pp. 140–198, MIT Press, Cambridge, Mass., 1996.

Hack, J. J., Parameterization of moist convection in the National Center for Atmospheric Research community climate model (CCM2), *J. Geophys. Res.*, *99*, 5541–5568, 1994.

Hao, W. M., and M.-H. Liu, Spatial distribution of tropical biomass burning in 1980 with 5° ×5° resolution, *Global Biogeochem. Cycles*, *8*, 495–503, 1994.

Hao, W. M., D. E. Ward, G. Olbu, and S. P. Baker, Emissions of CO_2, CO, and hydrocarbons from fires in diverse African savanna ecosystems, *J. Geophys. Res.*, *101*, 23,577–23,584, 1996.

Hauglustaine, D. A., G. P. Brasseur, S. Walters, P. J. Rasch, J.-F. Müller, L. K. Emmons, and M. A. Carroll, MOZART, a global chemical transport model for ozone and related chemical tracers, 2, Model results and evaluation, *J. Geophys. Res.*, *103*, 28,291–28,335, 1998.

Holtslag, A., and B. Boville, Local versus nonlocal boundary-layer diffusion in a global climate model, *J. Clim.*, *6*, 1825–1842, 1993.

Hough, A. M., Development of a two-dimensional global tropospheric model: Model chemistry, *J. Geophys. Res.*, *96*, 7325–7362, 1991.

Khalil, M. A. K., and R. A. Rasmussen, Global increase of atmospheric molecular hydrogen, *Nature*, *347*, 743–745, 1990.

Liousse, C., J. E. Penner, J. J. Walton, H. Eddleman, C. Chuang, and H. Cachier, Modeling biomass burning aerosols, in *Biomass Burning and Global Change*, edited by J. S. Levine, pp. 492–508, MIT Press, Cambridge, Mass., 1996.

Müller, J.-F., Geographical distribution and seasonal variation of surface emissions and deposition velocities of atmospheric trace gases, *J. Geophys. Res.*, *97*, 3787–3804, 1992.

Müller, J.-F., and G. P. Brasseur, IMAGES: A three-dimensional chemical transport model of the global troposphere, *J. Geophys. Res.*, *100*, 16,445–16,490, 1995.

Novelli, P. C., P. M. Lang, K. A. Masarie, D. F. Hurst, R. Myers, and J. W. Elkins, Molecular hydrogen in the troposphere: Global distribution and budget, *J. Geophys. Res.*, *104*, 30,427–30,444, 1999.

Olivier, J. G. J., A. F. Bouwman, C. W. M. van der Maas, J. J. M. Berdowski, C. Veldt, J. P. J. Bloos, A. J. H. Visschedijk, P. Y. J. Zandveld, and J. L. Haverlag, Description of EDGAR version 2.0, *RIVM Rep. 771060 002*, Natl. Inst. of Public Health and the Environ., Bilthoven, Netherlands, 1996.

Paneth, F. A., The chemical composition of the atmosphere, *Q. J. R. Metorol. Soc.*, *63*, 433–438, 1937.

Prinn, R. G., R. F. Weiss, B. R. Miller, J. Huang, F. N. Alyea, D. M. Cunnold, P. J. Fraser, D. E. Hartley, and P. G. Simmonds, Atmospheric trends and lifetime of CH_3CCl_3 and global OH concentrations, *Science*, *269*, 187–192, 1995.

Rotty, R. M., Estimates of seasonal variation in fossil fuel CO_2 emissions, *Tellus, Ser. B*, *39*, 184–202, 1987.

Schmidt, U., Molecular hydrogen in the atmosphere, *Tellus*, *26*, 78–90, 1974.

Schuler, S., and R. Conrad, Hydrogen oxidation activities in soil as influenced by pH, temperature, moisture, and season, *Biol. Fertil. Soils*, *12*, 127–130, 1991.

Seiler, W., and R. Conrad, Contribution of tropical ecosystems to the global budgets of trace gases, especially CH_4, H_2, CO, and N_2O, in *The Geophysiology of Amazonia: Vegetation and Climate Interactions*, edited by R. E. Dickerson, pp. 33–62, John Wiley, New York, 1987.

Simmonds, P. G., R. G. Derwent, S. O'Doherty, D. B. Ryall, L. P. Steele, R. L. Langenfelds, P. Salameh, H. J. Wang, C. H. Dimmer, and L. E. Hud-

son, Continuous high-frequency observations of hydrogen at the Mace Head baseline atmospheric monitoring station over the 1994–1998 period, *J. Geophys. Res.*, *105*, 12,105–12,121, 2000.

Warneck, P., *Chemistry of the Natural Atmosphere, Int. Geophys. Ser.*, vol. 41, 757 pp., Academic, San Diego, Calif., 1988.

Williamson, D. L., and P. J. Rasch, Two-dimensional semi-Lagrangian transport with shape preserving interpolation, *Mon. Weather Rev.*, *117*, 102–129, 1989.

Yonemura, S., S. Kawashima, and T. Tsuruta, Carbon monoxide, hydrogen, and methane uptake by soils in a temperate arable field and a forest, *J. Geophys. Res.*, *105*, 14,347–14,362, 2000.

D. H. Ehhalt, Institut für Atmosphärische Chemie, Forschungszentrum Jülich, D-52428 Jülich, Germany.

D. A. Hauglustaine, Service d'Aéronomie du CNRS, Université de Paris 6, 4, place Jussieu, boite 102, F-75252 Paris, France. (dh@aero.jussieu.fr)